A New Back-projection Algorithm in Frequency Domain for Multi-receiver Synthetic Aperture Sonar

Nguyen Dinh Tinh
Faculty of Radio-Electronic Engineering
Le Quy Don Technical University
Hanoi, Vietnam
tinhnd_k31@lqdtu.edu.vn

Trinh Dang Khanh
Faculty of Radio-Electronic Engineering
Le Quy Don Technical University
Hanoi, Vietnam
khanhtd_k31@lqdtu.edu.vn

***Abstract*— This paper proposes a new back-projection algorithm (BPA) based on the phase shifting in the frequency domain for multi-receiver synthetic aperture sonar (SAS) using linear frequency modulated (LFM) signal. With the consideration of the change of sound velocity in the depth, the Doppler effect, and the use of linearity property of inverse Fourier transform (IFT), the proposed BPA can improve the SAS image quality and reduce the computation time compared to the conventional BPA in the frequency domain. The improvements of the SAS image quality are represented by enhancing position accuracy, along-track resolution, the peak sidelobe ratio (PSLR), and signal/noise ratio (SNR). The merits of the proposed BPA are evaluated by comparing the simulation results from the proposed BPA and the conventional BPA with the sound velocity profile (SVP) in Vietnam's sea.**

Keywords*— *synthetic aperture sonar, multi-receiver, equivalent velocity, back-projection, SAS image, high-resolution.

I. Introduction

Synthetic aperture sonar (SAS) coherently combines consecutive pings along a known track to achieve the high azimuth (along-track) resolution, which is independent of the range and signal frequency [1]. Thanks to this capability, SAS has been widely used for many applications such as the search for small objects, underwater archaeology, and geological exploration [1-2]. Nowadays, SASs configured with an array of hydrophones combined with a transmitting projector, which are called the multi-receiver SAS, are commonly utilized to improve both the along-track resolution and the area coverage rate [3-4].

With the potential of generating high image quality, the back-projection algorithm (BPA) is usually used as a reference algorithm in the SAS image reconstruction [5-6]. The standard BPA (BPA in the time domain) using the interpolation, such as the interpolation based on *sinc* kernel function generates SAS images with the quality depending on interpolation accuracy [7]. To reduce the dependence of SAS image quality on interpolation accuracy, the BPA in the frequency domain is used for reconstructing SAS images [7]. This algorithm is named FT shifting BPA based on the characteristic of Fourier transform (FT) that the time delay in the time domain can be implemented by the phase shifting in the frequency domain [7, 8]. However, the conventional FT shifting BPA has ignored the change of sound velocity with depth and the Doppler frequency shift due to the continuous motion of the platform. With the restricted conditions, the SAS imaging performance can be degraded when coherently processing echo signals. In addition, the conventional FT shifting BPA expenses the huge computation load resulting from a large number of inverse Fourier transforms (IFT).

Based on the consideration of the variation of sound velocity with depth and the Doppler shift, and the utilization of the linearity property of IFT, this paper proposes a new FT shifting BPA enhancing the SAS imaging quality, reducing the computation load for multi-receiver SAS using linear frequency modulated (LFM) signal. The improvements of image quality consisting of the enhancement of position accuracy, along-track resolution, the peak sidelobe ratio (PSLR), and signal/noise ratio (SNR) are evaluated by comparing simulation results generated from the proposed FT shifting BPA and that yielded from the conventional FT shifting BPA. With the comparison of processing time for each algorithm in MATLAB, the enhancement of imaging efficiency derived by the proposed algorithm is also determined quantitatively.

II. Signal Model

A. Propagation Time And Equivalent Sound Velocity

The sound velocity in seawater is nonlinearly dependent on temperature, salinity, depth, and geographic coordinate. The change of sound velocity in depth can be described by the mathematical expression or the sound velocity profile (SVP) [9, 10]. The SVP in sea zones at a particular time can be obtained by sound velocity profilers.

With the variation of the sound velocity, acoustic refraction can occur. As a result, the sound rays can travel along curves or meanders. Fig.1 depicts a sound ray from A to B according to the meander generated by short straight lines. The sound is propagated along each straight line with a constant velocity. The propagation time from A to B is the total time in the short straights.

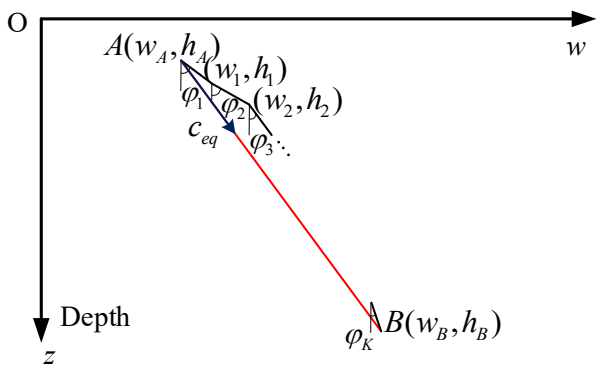

Fig. 1. Sound ray between two points

Applying Snell's law [10], the sound ray is expressed by:

$$\frac{\sin\varphi_{k+1}}{c_{k+1}} = \frac{\sin\varphi_k}{c_k} \quad (1)$$

The coordinates of the points on ray are given by:

$$w_1 = w_A + (h_1 - h_A) \times \tan\varphi_1 \tag{2}$$

…

$$w_B = w_A + \sum_{i=1}^{K} (h_i - h_{i-1}) \tan\left(\arcsin\left(\frac{c_i}{c_1} \sin\varphi_1 \right) \right) \tag{3}$$

where $h_0 = h_A$, $h_K = h_B$.

The propagation time from A to B is determined by:

$$\tau_\Sigma = \sum_{i=1}^{K} \frac{(h_i - h_{i-1})}{c_i \times cos\varphi_i} = \sum_{i=1}^{K} \frac{(h_i - h_{i-1})}{c_i \times \cos\left(\arcsin\left(\frac{c_i}{c_1} \sin\varphi_1 \right) \right)} \tag{4}$$

Based on the propagation time according to the meander, the equivalent sound velocity (ESV) is calculated by this propagation time for straight line AB, which is expressed as:

$$c_{eq} = \frac{AB}{\tau_\Sigma} = \frac{\sqrt{(h_B - h_A)^2 + (w_B - w_A)^2}}{\tau_\Sigma} \tag{5}$$

Expressions (3-5) show that the ESV is a function of the vertical inclination φ_1.

B. Signal Model for Multi-receiver SAS

Fig.2 shows the imaging geometry of a multi-receiver SAS consisting of a transmitter and receiver array with N uniformly spaced receivers by distance d. The distance between the transmitter and the ith receiver is d_i. The multi-receiver SAS linearly moves with constant velocity v in the azimuth dimension coinciding with the axis y. The axis x and h represent the range dimension (ground-range) and the depth dimension, respectively, and c_{eq} represents the ESV from (5).

With an ideal point target (pixel) located at $P(r,u,h)$, the position of the transmitter in the axis y is $u_T = vt$. The propagation time from the transmitter at T to the target at P during emission is determined as:

$$\tau_1 = \frac{\sqrt{(u - vt)^2 + r^2 + h^2}}{c_{eq\_T}} \tag{6}$$

where c_{eq_T} is the ESV during emission according to the vertical inclination φ_T.

$$\varphi_T \approx \arccos \frac{h}{\sqrt{(u - vt)^2 + r^2 + h^2}} \tag{7}$$

The angle between the motion direction of SAS and the sound propagation direction is α_1, which is given by [11]:

$$\alpha_1 = \arccos\left(\frac{u - vt}{\sqrt{(u - vt)^2 + r^2 + h^2}} \right) \tag{8}$$

When the signal arrives at point P, the scatter is generated in all directions, and the echo signal starts travelling to ith receiver at the direction $\overrightarrow{PR_i}$ determined by angle α_{2i} as:

$$\alpha_{2i} \approx \arccos\left(\frac{u - (d_i + v\tau_1 + vt)}{\sqrt{\left[u - (d_i + v\tau_1 + vt)\right]^2 + r^2 + h^2}} \right) \tag{9}$$

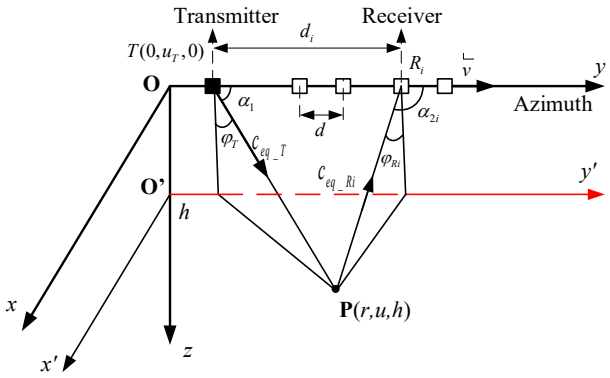

Fig. 2. Imaging geometry of multi-receiver SAS

The propagation time from point P to the ith receiver τ_{2i} satisfies the following equation:

$$\begin{aligned} c_{eq\_Ri}^2 \tau_{2i}^2 &= (u - vt)^2 + r^2 + h^2 + (d_i + v\tau_1 + v\tau_{2i})^2 \\ &\quad - 2\sqrt{(u - vt)^2 + r^2 + h^2}\,(d_i + v\tau_1 + v\tau_{2i}) \cos\alpha_1 \end{aligned} \tag{10}$$

where c_{eq_Ri} is the ESV during acquisition at the ith receiver according to the vertical inclination φ_{Ri} expressed as:

$$\varphi_{Ri} \approx \arccos \frac{h}{\sqrt{\left[u - (d_i + v\tau_1 + vt)\right]^2 + r^2 + h^2}} \tag{11}$$

From (10), τ_{2i} is determined by:

$$\tau_{2i} = \frac{v\left(d_i + v\tau_1 - \sqrt{(u - vt)^2 + r^2 + h^2} \times \cos\alpha_1\right) + \sqrt{\Delta_i}}{c_{eq\_Ri}^2 - v^2} \tag{12}$$

where Δ_i is the discriminant of the quadratic equation (9), which is expressed as below:

$$\begin{aligned} \Delta_i &= v^2 \left(d_i + v\tau_1 - \sqrt{(u - vt)^2 + r^2 + h^2} \times \cos\alpha_1\right)^2 \\ &\quad + \left(c_{eq\_Ri}^2 - v^2\right) \left(\begin{aligned} &(u - vt)^2 + r^2 + h^2 + (d_i + v\tau_1)^2 \\ &- 2\sqrt{(u - vt)^2 + r^2 + h^2}\,(d_i + v\tau_1) \cos\alpha_1 \end{aligned} \right) \end{aligned} \tag{13}$$

With the common utilization of wideband waveforms such as the LFM signals [5-7, 12], the transmitted signal can be expressed as below:

$$p(\tau) = \mathrm{w}(\tau) \exp\left(j2\pi f_0 \tau + j\pi\gamma\tau^2 \right) \tag{14}$$

where τ represents the fast time in the slant range dimension, f_0 is the center frequency, γ is the chirp rate [Hz/s]. $\mathrm{w}(\tau)$ expresses the signal amplitude defined as [6, 13]:

$$w(\tau) = rect\left(\frac{\tau}{T_p} \right) = \begin{cases} 1, & |\tau / T_p| \le 0.5 \\ 0, & \text{otherwise.} \end{cases} \tag{15}$$

where T_P is the pulse duration (pulse length) of the transmitted signal.

The echo signals received at the ith receiver due to the scatters from point P are determined as [12, 14]:

$$\begin{aligned} s_i(\tau, t) &= \sigma_i(t)\, \omega_{Ri}(t)\, \mathrm{w}\left[\eta_{2i}\eta_1(\tau - \tau_{2i}) - \eta_1\tau_1\right] \\ &\quad \times \exp\left\{ \begin{aligned} &j2\pi f_0 \left[\eta_{2i}\eta_1(\tau - \tau_{2i}) - \eta_1\tau_1\right] \\ &+ j\pi\gamma \left[\eta_{2i}\eta_1(\tau - \tau_{2i}) - \eta_1\tau_1\right]^2 \end{aligned} \right\} \end{aligned} \tag{16}$$

where $\omega_{Ri}(t)$ denotes the product of the transmitter beam and the *i*th receiver beam, which is suppressed for simplicity. $\sigma_i(t)$ represents the reflection coefficient in the direction from point P to the *i*th receiver. To simplify the calculation, the target has a similar reflection coefficient in all directions. η_1 and η_{2i} are the time-stretching factors of the signals received at point P and the *i*th receiver due to the Doppler effect, respectively, which are expressed as below:

$$\eta_1 = \frac{c}{c - v\cos\alpha_1} \tag{17}$$

$$\eta_{2i} = \frac{c + v\cos\alpha_{2i}}{c} \tag{18}$$

With the above conditions of the beam pattern and the reflection coefficient, the expression (16) can be reformed as:

$$s_i(\tau,t) = \mathrm{w}\left(\eta_1\eta_{2i}\left(\tau-\tau_{imo}\right)\right)\exp\left(\begin{matrix} j2\pi f_0\eta_1\eta_{2i}\left(\tau-\tau_{imo}\right) \\ +j\pi\gamma\left(\eta_1\eta_{2i}\left(\tau-\tau_{imo}\right)\right)^2 \end{matrix}\right) \tag{19}$$

where τ_{imo} is the modified signal propagation time, which is determined as below:

$$\tau_{imo} = \frac{\tau_1}{\eta_{2i}} + \tau_{2i} \tag{20}$$

The modified signal propagation time τ_{imo} represents not only the amount of signal delay but also the phase change due to the Doppler shift.

III. PROPOSED FT SHIFTING BPA

The BPA is called Delay-And-Sum or the correlation algorithm in SAS systems using broadband signals [1, 3]. The FT shifting BPA is performed based on the phase shifting in the frequency domain instead of the phase shifting in the time domain [7-8]. The conventional FT shifting BPA includes steps of the transformation of the received signals into the frequency domain using FT, the range compression (match filtering), the phase shifting in the frequency domain based on the range cell migration (RCM), the data transformation into the time domain via IFT [7]. After storing the data, the coherent superposition and the max are performed to obtain the image of each pixel [3, 7].

With the conventional FT shifting BPA, the signal propagation time is determined by suppressing the change of sound velocity in the depth and ignoring the Doppler effect. It is determined according to the point $P_n(r_n,u_n,h)$ as [6, 7]:

$$\tau_i(r_n,u_n) = \frac{v\left(\left(vt-u_n\right)+d_i\right)+c_0\sqrt{\left(vt-u_n\right)^2+r_n^2+h^2}}{c_0^2-v^2} + \frac{\sqrt{\left[v\left(vt+d_i-u_n\right)+c\sqrt{\left(vt-u_n\right)^2+r_n^2+h^2}\right]^2+\left(c^2-v^2\right)\left(2\left(vt-u_n\right)d_i+d_i^2\right)}}{c_0^2-v^2} \tag{21}$$

where c_0 is a constant value chosen by 1500 m/s [7, 13], or the average sound velocity between vehicle and seafloor, or the sound velocity at the SAS depth [15].

After coherently processing, the target function for the target located at $P_n(r_n,u_n)$ in the plane Oxy is expressed as [7]

$$ff(x,r_n,u_n) = \sum_{m=1}^{M}\sum_{i=1}^{N} F^{-1}\left[S_i(f_\tau,t)P^*(f_\tau)\exp\left(j2\pi f_\tau\Delta\tau_i\right)\right] \tag{22}$$

where F^{-1} denotes the IFT in the slant range dimension, *M* is the number of pulse repetition intervals (pings) when coherently integrating, $S_i(f_\tau)$ is the FT of signals $s_i(\tau, t)$ shown in (19), $P^*(f_\tau)$ is the conjugated spectrum of the transmitted signal represented in (14), f_τ is the instantaneous frequency corresponding to the fast time when the sample satisfies the Nyquist frequency. $\Delta\tau_i$ denotes the time delay of the echo signal at the *i*th receiver, which is given by [7]

$$\Delta\tau_i = \tau_i - 2\frac{\sqrt{r_n^2+h^2}}{c_0} \tag{23}$$

With the difference from the sound velocity and the suppression of the Doppler effect, the SAS image quality achieved by using conventional FT shifting BPA may be degraded. Moreover, to coherently process the received signals at *N* receivers in *M* pings, the conventional FT shifting BPA requires *NM* the IFTs and the range compressions for each pixel in the azimuth dimension. With the huge number of IFTs and range compressions, the computation load via the conventional BPA is considerably increased when reconstructing SAS images with large sizes.

By exploiting the linearity property of IFT that is the same as the linearity property of FT [8], expression (22) can be reformulated as:

$$\begin{aligned} ff(x,r_n,u_n) &= F^{-1}\left\{\sum_{m=1}^{M}\sum_{i=1}^{N} S_i(f_\tau)P^*(f_\tau)\exp\left(j2\pi f_\tau\Delta\tau_i\right)\right\} \\ &= F^{-1}\left\{P^*(f_\tau)\left[\sum_{m=1}^{M}\sum_{i=1}^{N} S_i(f_\tau)\exp\left(j2\pi f_\tau\Delta\tau_i\right)\right]\right\} \end{aligned} \tag{24}$$

The conjugated spectrum of the transmitted signal can be drawn from the two summations due to its independence with *i* and *m*.

Based on these mathematical transformations, the IFT and the range compression can be carried out after the coherent superposition. Therefore, the number of IFT and range compression for the proposed BPA is mitigated to 1 instead of *NM* for the conventional BPA by swapping the order of calculations.

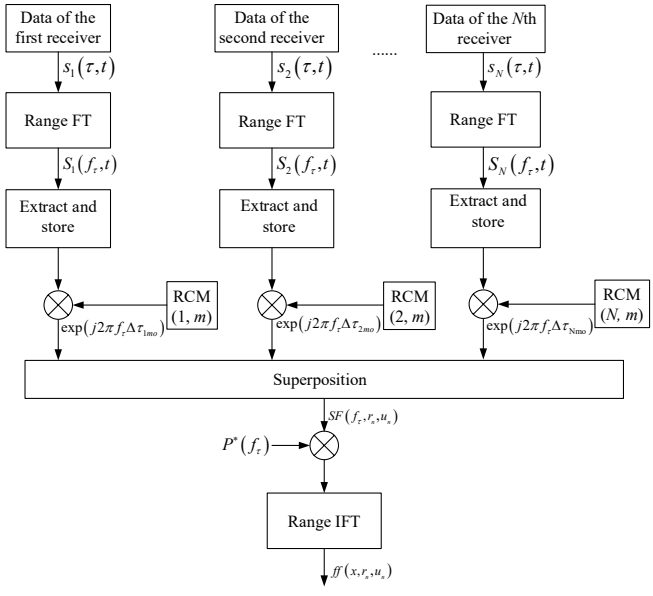

Fig. 3. Block diagram of proposed FT shifting BPA

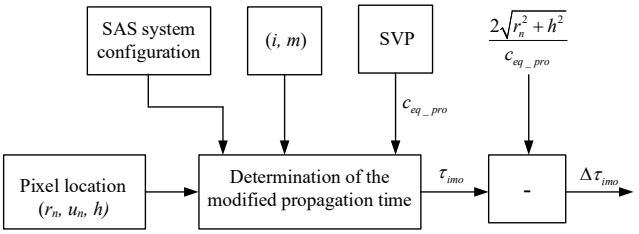

Fig. 4. Block diagram of the RCM processor from proposed BPA

With the utilization of the modified signal propagation time τ_{imo} and the mathematical transformations reducing the numbers of IFT and range compression, a block diagram of the proposed BPA is depicted as in Fig. 3. The block diagram of the RCM processor for calculating the modified signal delays is shown in Fig. 4.

Indifference to the conventional FT shifting BPA, the modified signal delay at the ith receiver determined by the proposed BPA is modified as:

$$\Delta\tau_{imo}\left(r_n,u_n\right)=\tau_{imo}\left(c_{eq\_pro}\right)-2\frac{\sqrt{r_n^2+h^2}}{c_{eq\_pro}} \tag{25}$$

where c_{eq_pro} is the equivalent velocity for coherently processing echo signals. In order to simply in the calculation, c_{eq_pro} is chosen as the average of the maximum ESV value $c_{eq\_\max}$ and the minimum ESV value $c_{eq\_\min}$ over the variety of vertical inclinations.

$$c_{eq\_pro}=\left(c_{eq\_\max}+c_{eq\_\min}\right)/2 \tag{26}$$

After the superposition, the summation data is determined as below:

$$SF\left(f_\tau,r_n,u_n\right)=\sum_{m=1}^{M}\sum_{i=1}^{N}S_i\left(\mathrm{f}_\tau,t\right)\exp\left(j2\pi f_\tau\Delta\tau_{imo}\right) \tag{27}$$

The target function for the target located at $P_n\left(r_n,u_n\right)$ achieved by the proposed FT shifting BPA is given by:

$$ff\left(x,r_n,u_n\right)=F^{-1}\left[SF\left(f_\tau,r_n,u_n\right)P^*\left(f_\tau\right)\right] \tag{28}$$

When changing the focus point in the azimuth dimension, the expression (28) generates a function of two variables $\gamma(x,y)$. With the input data from an ideal point target, $\gamma(x,y)$ is the point target response (or the point spread function (PSF)) [13, 16, 17]. The image quality is measured by analyzing the PSF with parameters: the peak position (or the accuracy position), along-track resolution, PSLR, and the peak amplitude (or SNR) [16]. The parameters can be determined in the azimuth dimension by maximizing $ff\left(x,r_n,u_n\right)$ with the variable x and plotting the beam pattern according to the variable y (azimuth slice).

IV. Simulation Results

To highlight the effectiveness of the proposed FT shifting BPA, the study considers an example of multi-receiver SAS with the parameters expressed in Table 1. In this system, the distance between two adjacent receivers is also the length of one receiver (or one transmitter) in the azimuth dimension. The platform velocity is chosen to avoid grating lobes of the synthetic beam pattern [1, 3].

TABLE I. The SAS System Parameters

Parameters	Value	Units
Center frequency (carrier frequency) (f_0)	100	kHz
Signal bandwidth (Δf)	20	kHz
Pulse length (T_P)	10×10^{-3}	s
Pulse repetition interval (T_R)	0.21	s
Platform velocity (v)	1.5	m/s
Distance from the transmitter to the first receiver element (d_1)	0.03	m
Distance between two adjacent receivers (d)	0.02	m
Number of receivers (N)	32	element

Fig. 5 shows SVP obtained from Vietnam's sea zone at (017°03'09''N, 107°27'17''E) in April 2021 by a sound velocity profiler (SWiFT SVP) of Valeport Ltd. When the SAS depth and the target depth are 3 m and 45 m, respectively, the depth from SAS to the target (h) is 42 m.

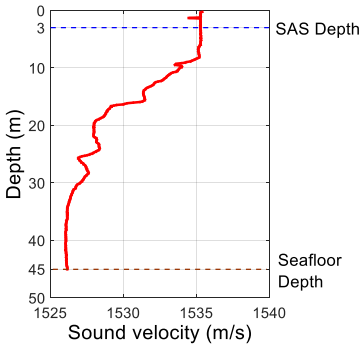

Fig. 5. Sound velocity profile at (017°03'09''N, 107°27'17''E)

With the pulse repetition interval T_R = 0.21 s, the slant range can be chosen as 150 m. The maximum vertical inclination is calculated as:

$$\varphi_{\max}=arc\cos\frac{42}{150}\approx74^\circ \tag{29}$$

The values of ESV depending on the vertical inclination with SVP from Fig.5 are depicted as Fig. 6. From this figure, EVS gradually changes from 1529.127 m/s to 1529.167 m/s in the scope of vertical inclinations investigated. Therefore, the EVS for coherently processing signals is 1529.147 m/s.

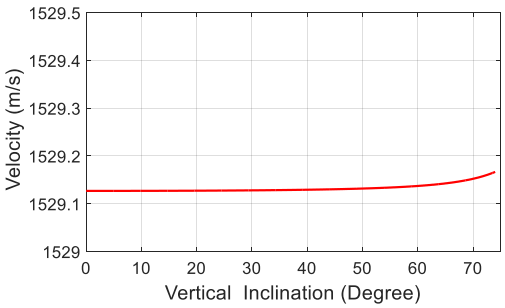

Fig. 6. Dependence of equivalent sound velocity on the vertical inclination

Consider an ideal point target located at (132 m, 11 m) in the plane Oxy. The number of pings is 120, which is chosen to ensure that the main beams of each receiver element overlap at the target position.

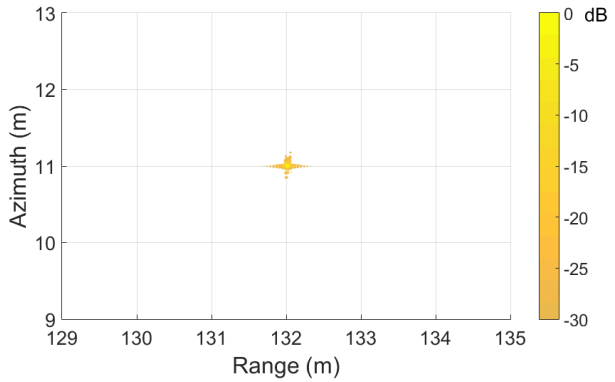

Fig. 7. Point spread function of the point target at (132 m, 11 m) from the proposed BPA

Fig. 7 expresses PSF from the proposed FT shifting BPA, also describes the focusing result for the point target. Inspecting Fig.7, the proposed FT shifting BPA can provide a focused image at the target position.

Two azimuth slices from the proposed BPA and the conventional BPA (c_0 = 1535.27 m/s, the sound velocity at the SAS depth) for the above ideal point target are expressed as Fig. 8. In this figure, the red solid curve and the blue dashed curve depict results from the proposed BPA and the conventional BPA, respectively.

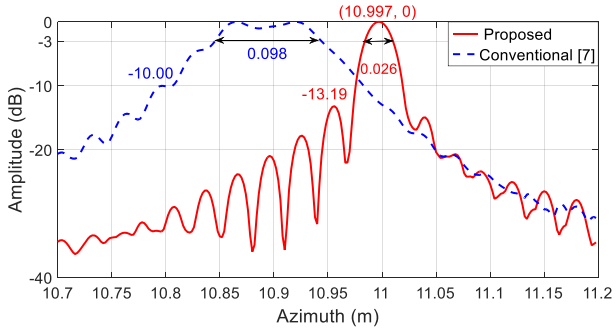

Fig. 8. Azimuth slices of the point target

In order to calculate the deviations, the target positions are determined according to the midpoints of the main beams. With the proposed BPA, the deviation approximately equals 0.003 m, whereas that is 0.105 m by using the conventional BPA. Owning to the sound velocity error from the real value and the suppression of the Doppler effect, the deviation from the conventional BPA is much larger than from the proposed BPA.

From Fig. 8, the along-track resolutions (3 dB) and PSLR obtained from the proposed BPA are significantly improved compared with that from the conventional BPA. The along-track resolution raised by the proposed BPA is 2.6 cm, whereas that derived by the conventional BPA is 9.8 cm. Besides, the proposed BPA decreases PSLR by more than 3 dB in comparison with the conventional BPA.

To evaluate the improvement of SNR achieved by the proposed BPA compared with the conventional BPA, the two azimuth slices obtained from the two algorithms are normalized according to the same maximum value (named relative normalization). The relative normalized azimuth slices of the above target are represented in Fig. 9.

In Fig. 9, the peak levels of the main beam (also SNR) raised by the proposed BPA are larger than nearly 5.6 dB compared with by the conventional BPA. With the SNR enhancement, the SAS image quality obtained from the proposed algorithm is considerably improved in comparison to the conventional algorithm.

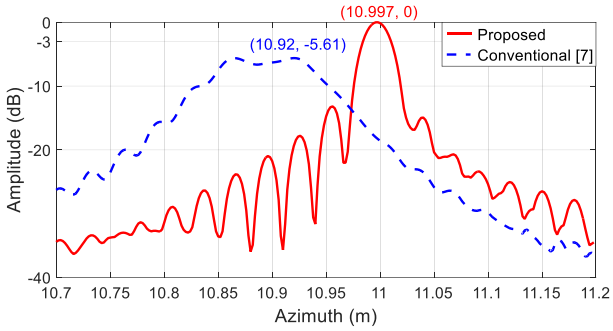

Fig. 9. Relative normalized azimuth slices of the point target

To evaluate the computation load of the two BPAs, the study tests computation time for the two algorithms in MATLAB 2015A on a laptop with an i7-1065G7 Intel processor, 8 GB RAM. The processing time of the two algorithms after the FT for each pixel is determined by the average value of 10 simulations. With 120 pings, the average times for the proposed BPA and the conventional BPA are 16.565 s and 20.748 s, respectively. Despite the consideration of the change in sound velocity with depth and the Doppler effect, the proposed BPA consumes less processing time than the conventional BPA due to the mitigation of the number of IFTs and range compressions. The reduction of the processing time is approximately 1.3 times for 120 pings. However, the processing time of the proposed BPA is still heavy for real-time applications. This issue can be solved using more powerful computing devices than ours.

V. Conclusion

This paper has proposed an FT shifting BPA that has improved the image quality by mitigating the deviation of the azimuth coordinate, reducing PSLR, enhancing the along-track resolution, and increasing the SNR in comparison with the conventional FT shifting BPA. Furthermore, with the reduction of the number of IFTs and range compressions, the proposed BPA also has shortened the processing time compared with the conventional BPA. The imaging results and calculating results have illustrated the improvements in image quality and the computation time derived from the proposed algorithm with the real data of SVP in Vienam's sea.

References

[1] N. Kolev, "Sonar Systems," InTech Croatia, pp.3-25, 2011.

[2] R. E. Hansen, "Synthetic Aperture Sonar Technology Review," Marine Technology Society Journal, vol. 47, no. 5, pp.117-127, October 2013.

[3] M. P. Hayes and P. T. Gough, "Synthetic Aperture Sonar: A Review of Current Status," in IEEE Journal of Oceanic Engineering, vol. 34, no. 3, pp. 207-224, July 2009, doi: 10.1109/JOE.2009.2020853.

[4] N. D. Tinh and T. Dang Khanh, "A New Imaging Geometry Model for Multi-receiver Synthetic Aperture Sonar Considering Variation of The Speed of Sound in Seawater," IEIE Transactions on Smart Processing & Computing, Vol.10, No.04, pp.302-308, August 2021, https://doi.org/10.5573/IEIESPC.2021.10.4.302.

[5] X. Zhang, J. Tang and H. Zhong, "Multi-receiver Correction for the Chirp Scaling Algorithm in Synthetic Aperture Sonar," in IEEE Journal

of Oceanic Engineering, vol. 39, no. 3, pp. 472-481, July 2014, doi: 10.1109/JOE.2013.2251809.

[6] Zhang, X.; Huang, H.; Ying, W.; Wang, H.; Xiao, “J. An indirect range-Doppler algorithm for multi-receiver synthetic aperture sonar based on Lagrange inversion theorem,” IEEE Trans. Geosci. Remote Sens. 2017, 55, 3572–3587, doi: 10.1109/TGRS.2017.2676339.

[7] X. Zhang, P. Yang, C. Tan and W. Ying, "BP algorithm for the multi-receiver SAS," IET Radar Sonar Navig., vol. 13, iss. 5, pp. 830-838, February 2019, https://doi.org/10.1049/iet-rsn.2018.5468.

[8] B.R. Mahafza, and A. Elsherbeni, “MATLAB Simulations for Radar Systems Design,” Chapman & Hall/CRC CRC Press LLC, Chapter 13, 2004.

[9] P. C. Etter, “Underwater acoustic modeling and simulation,” fourth edition Taylor & Francis Group, pp. 28-35, 2013.

[10] A. D. Waite, “Sonar for practising Engineers,” John Wiley & Sons Ltd, England, pp. 51- 60, 2002.

[11] N. D. Tinh and T. Dang Khanh, "A New Imaging Geometry Model for Determining Phase Distribution in Multi-receiver Synthetic Aperture Sonar," 2019 6th NAFOSTED Conference on Information and Computer Science (NICS), 2019, pp. 518-521, doi: 10.1109/NICS48868.2019.9023897.

[12] S. Pinson, and C.W. Holland, "Relative velocity measurement from the spectral phase of a match-filtered linear frequency modulated pulse," J. Acoust. Soc. Am, vol. 140, Iss. 2, pp. 191-196, Aug. 2016.

[13] Yan Pailhas, Samantha Dugelay, and Chris Capus , "Impact of temporal Doppler on synthetic aperture sonar imagery," The Journal of the Acoustical Society of America 143, 318-329 (2018) https://doi.org/10.1121/1.5021250.

[14] D. W. Hawkins and P. T. Gough, “Temporal Doppler effects in SAS,” Proc. Inst. Acoust. **26**(5), pp.1-10, 2004.

[15] R. E. Hansen, T. O. Sæbø, J. C. Hayden, P. E. Hagen, "The SENSOTEK Synthetic Aperture Sonar - results from HUGIN AUV trials," Norwegian Defence Research Establishment (FFI), pp. 19-21, June 2007.

[16] Cumming, I., Wong, F., “Digital Processing of Synthetic Aperture Radar Data: Algorithms and Implementation,” Artech House, 2005, Chapter 2.

[17] Angeliki Xenaki and Yan Pailhas , "Compressive synthetic aperture sonar imaging with distributed optimization," The Journal of the Acoustical Society of America 146, 1839-1850 (2019) https://doi.org/10.1121/1.5126862.